ACS OMEGA

Open Access

http://pubs.acs.org/journal/acsodf

Article

Fluorescent Probes Based on 7-(Diethylamino)quinolin-2(1*H*)-one Cucurbit[7]uril Complexes for Indicator Displacement Assays: *In Silico* and Experimental Approaches

Kevin Droguett, Guillermo E. Quintero, Nuno Basilio, Angélica Fierro, Edwin G. Pérez, and Margarita E. Aliaga*

Cite This: *ACS Omega* 2025, 10, 27550−27558

Read Online

ACCESS | Metrics & More | Article Recommendations | Supporting Information

ABSTRACT: In this work, two 7-(diethylamino)quinolin-2(1*H*)-one derivatives (**DQ1** and **DQ2**) were synthesized and characterized both structurally and physicochemically. The interaction of these derivatives with cucurbit[7]uril (**CB7**) was explored through combined experimental and *in silico* approaches, highlighting their unique behavior and practical potential. Experimentally, the complexes exhibited a 1:1 stoichiometry, as confirmed by fluorescence spectroscopy and isothermal titration calorimetry (ITC). Remarkably, the interaction with the **CB7** macrocycle resulted in an unusual negative shift in the pK_a values of the probes alongside a significant enhancement in fluorescence emission, quantum yield, and fluorescence lifetime. From a computational perspective, the molecular dynamics simulations (MD) demonstrated that hydrogen bonds play a critical role in maintaining the system's stability. Finally, **DQ2** is proposed as a probe for the indicator displacement assay (IDA) and was tested using methyl viologen (**MV**) as an analyte.

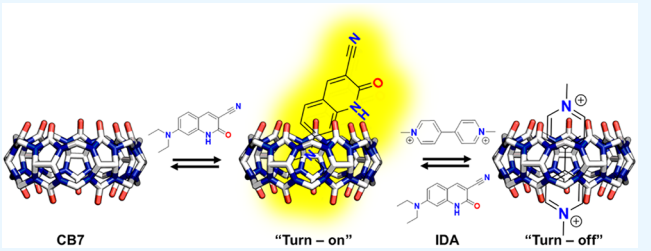

INTRODUCTION

In recent years, supramolecular chemistry has garnered significant attention for various applications.[1−4] Host−guest inclusion complexes comprise a particular class of supramolecular binding pairs, which have been widely used to construct functional self-assembled architectures. These assemblies involve noncovalent bonding between a host, often a larger structure such as a macrocycle, and a guest molecule that inserts into the host cavity. The inclusion of guest molecules in these confined spaces often results in the modulation of their physicochemical properties relative to those observed in bulk solutions. Commonly employed macrocycles to form host−guest complexes include cyclodextrins,[5] calixarenes,[6] pillararenes,[7] and cucurbiturils.[8] Notably, cucurbit[7]uril (**CB7**) has attracted significant interest as a high-affinity host receptor with various applications due to its favorable characteristics, including adequate water solubility, biocompatibility, symmetry, low polarizability, and the presence of a hydrophobic cavity with hydrophilic portals.[9] These properties make **CB7** a versatile host for numerous applications, including catalysis,[10,11] drug delivery,[12] photodynamic therapy,[13] molecular recognition,[14] and sensing.[15]

It is noteworthy that the applicability of **CB7** is directly dependent on the specific objectives of the study, which guide the selection of the guest. Consequently, numerous inclusion complexes involving **CB7** have been reported, with guests ranging from metal cations[16] and small organic molecules, such as aliphatic diamine derivatives,[17] cyclopentadiene,[10] and cyclohexane,[18] to larger molecules like coumarins,[19] quinoxalinones,[20] and berberines.[21] Despite the wide range of structures capable of forming inclusion complexes with **CB7**, quinoline-2(1*H*)-one derivatives have not been extensively studied from a theoretical or experimental perspective. This family of molecules is aza-analogues of coumarins, with well-documented antibacterial and antifungal properties.[22−26] Moreover, these derivatives are more thermally and chemically[27] stable than coumarins, with different optical responses.[28] Furthermore, incorporating electron-donating group (EDG) and electron-withdrawing group (EWG) into these rings modulates their photophysical properties.[29,30] In the case of EDG, such as diethylamino (−NEt_2), and EWG, such as carbaldehyde (−CHO), promote changes in the photophysical behavior of these compounds. An illustrative example is the compound 7-(diethylamino)quinolin-2(1*H*)-one-3-carbaldehyde (**DQ1**) (see Figure 1), which contains these functional groups.[31] A carbaldehyde substituent within

Received: April 16, 2025
Revised: May 13, 2025
Accepted: June 9, 2025
Published: June 17, 2025

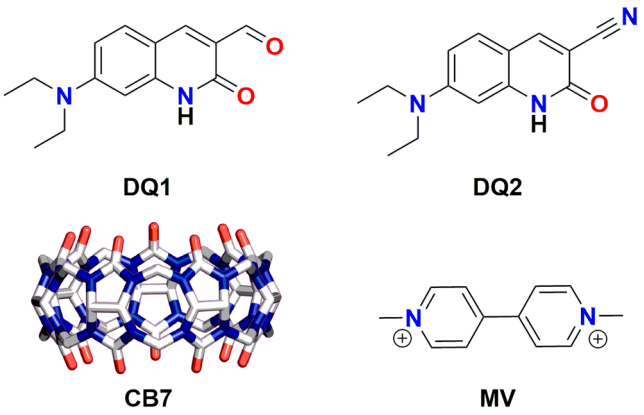

Figure 1. Chemical structures of dyes **DQ1** and **DQ2**, the macrocycle **CB7**, and the competitive guest **MV** employed in this work.

the ring facilitates electronic delocalization and enables the modification of the EWG, such as carbonitrile (−CN),[32] or the addition of other molecular fragments.[30,33] The presence of this type of substituent on the quinolin-2(1*H*)-one ring modifies its photophysical properties, which favors the formation of new fluorescent probes. However, their potential[34] as fluorescent probes, as well as the supramolecular effects induced by **CB7** on properties such as pK_a, absorbance, emission spectra, fluorescence quantum yields, and lifetimes, has not been explored. While several studies have reported the formation of inclusion complexes between **CB7** and coumarin derivatives with binding constants in the range of 10^5−10^7 M^{-1},[19,35−38] it seems reasonable to hypothesize that similar structures, such as quinolin-2(1*H*)-ones, would also form inclusion complexes with **CB7**. However, no evidence has been presented to confirm such an association.

In this work, we investigated the encapsulation of 7-(diethylamino)quinoline-2(1*H*)-one-3-carbaldehyde (**DQ1**) and 7-(diethylamino)quinoline-2(1*H*)-one-3-carbonitrile (**DQ2**) in the **CB7** cavity (see Figure 1) and the modulation of their properties. Furthermore, we examined the binding thermodynamics to gain insight into the driving force of the complexation. Finally, we studied the use of these quinoline-2(1*H*)-one derivatives in an indicator displacement assay (IDA) to determine a highly accurate binding constant of 1,1'-dimethyl-4,4'-bipyridinium (**MV**) toward **CB7**.

RESULTS AND DISCUSSION

Physical organic chemistry studies are important for the development of new colorimetric and fluorescent probes for indicator displacement assays (IDA).[39] To this end, we synthesized and characterized two quinolinone derivatives (Scheme 1, Figures S1−S8 and Tables S1-S4). Moreover, the photophysical characterization of the probes is summarized in Table 1. In particular, Figure 2 shows the absorption spectra of both quinoline-(2*H*)-one derivatives. **DQ1** has a band centered at 430 nm with a molar absorptivity coefficient (ε) of 4.0 × 10^4 L mol^{-1} cm^{-1}, which corresponds to a $\pi\rightarrow\pi^*$ transition. Similarly, the $\pi\rightarrow\pi^*$ band of **DQ2** is centered at 409 nm. These findings align well with previously reported spectral characteristics of quinolinones and coumarin derivatives, supporting the consistency of their electronic structures and photophysical behavior. The similarity in their absorption bands suggests that both probes possess conjugated systems capable of efficient $\pi\rightarrow\pi^*$ transitions, likely influenced by their molecular frameworks and substituent effects

In the presence of the macrocycle **CB7**, **DQ1** and **DQ2** exhibited bathochromic shifts in their absorbance spectra of 4 and 7 nm shifts in their emission maxima, respectively. Significant changes were observed in the fluorescence quantum yield and fluorescence lifetimes (see Table 1 and Figures S13 and S14). For **DQ1**, quantum yields increased 5-fold, while **DQ2** demonstrated an exceptional enhancement from 0.03 to 0.54, corresponding to an 18-fold increase in the presence of **CB7**. This improvement in the ϕ_f of **DQ2** highlights the profound impact of **CB7** as a host molecule. Such effects have been extensively reported for various molecular systems, where **CB7** enhances ϕ_f by stabilizing the intramolecular charge-transfer (ICT) state.[40−42] This stabilization inhibits the formation of the twisted intramolecular charge-transfer (TICT) state, a nonradiative pathway that typically competes with radiative deactivation. Consequently, **CB7** promotes radiative decay, thereby significantly enhancing the fluorescence efficiency of the guest molecules. These findings underscore the potential of **CB7** in designing highly fluorescent systems for sensing, imaging, and molecular recognition applications.

The fluorescence lifetimes exhibited differences between the two probes. **DQ1** did not exhibit a measurable time decay under the experimental conditions due to a poor fit in the reconvolution analysis; however, it can be inferred that the fluorescence time decay is less than 0.02 ns. In contrast, **DQ2** presented two distinct fluorescence lifetimes: τ_1 attributed to the locally excited state (LE), and τ_2 assigned to the intramolecular charge transfer state, with the second lifetime (3.64 ns) contributing most significantly. Notably, **DQ2** in water exhibited high fluorescence lifetimes and ϕ_f, which can be attributed to the −CN substituent. The nitrile group is a stronger EWG than the −CHO substituent, which improves the photophysical properties of **DQ2** and allows it to be applied as a fluorescent probe.

The complexes formed between the quinoline-2(1*H*)-one derivatives and macrocycle **CB7** were studied by spectroscopic means. First, the formation of complexes **DQ***n*•**CB7** leads to an increase in the ϕ_f of both probes and stabilizes their second lifetime (see Table 1). This can be attributed to the inhibition of the TICT state of the −NEt_2 moiety,[43] thus promoting the planarity of the probes and enhancing their photophysical activity. Furthermore, the above leads to an increase in the fluorescence intensity of the probes upon the addition of the macrocycle, which allowed us to conveniently determine the

Scheme 1. Synthesis of DQ1 and DQ2

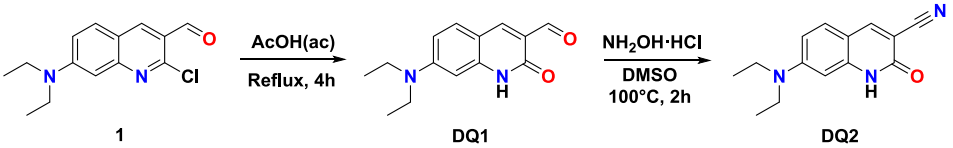

https://doi.org/10.1021/acsomega.5c03501
ACS Omega 2025, 10, 27550−27558

Table 1. Spectroscopic Data of DQ1 and DQ2 and Their Complexes with CB7

	λ_{max}^{abs} (nm)	λ_{max}^{emi} (nm)	ε (L mol^{-1}cm^{-1})	ϕ_f	τ_1 (B1)/ns	τ_2 (B2)/ns
DQ1	430	499	40000	0.009	<0.02	–
DQ1•CB7	434	495	42800	0.049	0.11 (43.97)	0.32 (55.97)
DQ2	409	456	47500	0.030	0.13 (27.92)	3.64 (72.08)
DQ2•CB7	416	458	47800	0.540	1.21 (13.68)	3.56 (86.32)

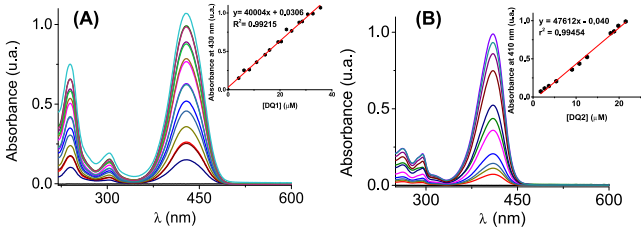

Figure 2. Absorbance spectra of (A) **DQ1** and (B) **DQ2**, in water with 1% of ACN as cosolvent. The inset shows the dependence of concentration with the absorbance at the maximum wavelength for each probe (430 nm and 410 nm, respectively).

binding affinity for the complexes, as shown in Figure 3. Both probes have remarkable affinity constants toward **CB7** in the

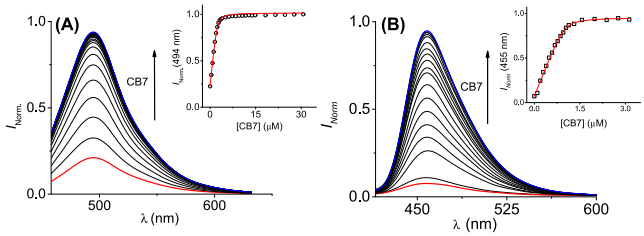

Figure 3. Fluorescent intensity dependence of (A) **DQ1** (1.6 μM) upon the addition of **CB7** (0–70 μM) and (B) **DQ2** (1 μM) upon the addition of **CB7** (0–3 μM). The inset shows the fit for a 1:1 stoichiometry complex (A) (K_b: 7.5 ± 0.8 × 10^6 M^{-1}) and (B) (K_b: 1.1 ± 0.1 × 10^7 M^{-1}). Milli-Q water:ACN (99:1) at 25 °C, pH = 5.86.

order of 10^7 M^{-1}, which can be useful for their use in indicator displacement assays (IDAs). It is important to note that for those assays, the analyte of interest needs to be in the range given by the equation:[44]

$$\log K^{HI} + 1 \geq \log K^{HG} \geq \log K^{HI} - 2 \quad (1)$$

where K^{HI} is the probe's binding constant, in this case, the quinoline-2(1*H*)-one derivative, and K^{HG} is the constant of the guest of interest. Considering this, the potential analytes for the IDA should be in the range of 10^5 and 10^8 M^{-1} binding constants toward **CB7** to perform an adequate binding constant determination.

After that, the pK_a values of the quinoline-2(1*H*)-one derivatives and their host–guest complexes with **CB7** were determined from the absorption spectra recorded at different pH values. As can be observed from Figure 4, both **DQ1** and **DQ2** showed complexation-induced negative pK_a shifts. It is worth noting that negative shifts are very unusual for **CB7** host–guest complexes, though they have been reported for some compounds with –NEt$_2$ substituents.[45,46] Moreover, the ^{1}H NMR spectra (see Figures S9 and S10) presented similar chemical shift displacements for both adducts in the presence of the macrocycle, which suggests a similar binding position inside the cucurbituril. The evidence presented suggests that

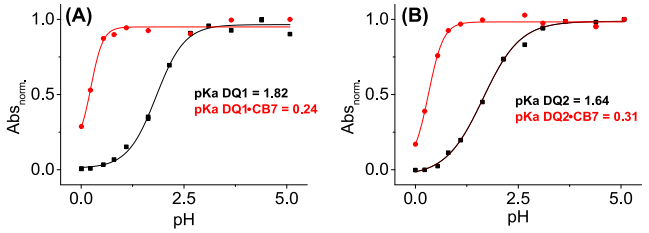

Figure 4. pH titrations of (A) **DQ1** (1 μM) black line and dots and the complex **DQ1•CB7** (20 μM of macrocycle) red line and dots and (B) **DQ2** (1 μM) black line and dots and the complex **DQ2•CB7** (20 μM of macrocycle) red line and dots in water:ACN (99:1) at 25 °C.

CB7 stabilizes the neutral compound over its protonated counterpart when the –NEt$_2$ substituent is present.

In order to gain further insights into the conformation of the complexes, we conducted molecular dynamics simulations for both systems in explicit water under NTP conditions. The MD results show that both complexes remain stable during the 300 ns simulation (RMSD < 1.5 Å), and a hydrogen bond network contributes to system stabilization (see Figures S3 and S4). Additionally, the conformations of the complexes can be seen in Figure 5, where both complexes show similar behavior.

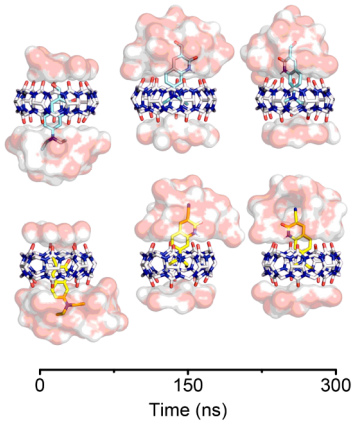

Figure 5. Conformations of (A) **DQ1** and (B) **DQ2** inside **CB7** during a 300 ns MD study. The water molecules interacting with the probes and the macrocycle are shown as a surface.

Initially, the quinoline-2(1*H*)-one derivatives are included by the lactam fraction of the molecules; however, as the simulation progresses, the –NEt$_2$ moiety enters the hydrophobic cavity of the macrocycle. Thus, the hydrophilic fraction of the quinolinones is exposed to the solvent, and a hydrogen bond between the N–H of the lactam fraction and the oxygen from the carbonylic portal of the macrocycle is favored. Considering this, the MD simulation suggests that both quinolinones bind similarly to **CB7** in the ground state. Alongside this result is the NMR shift observed in S9 and S10, where an approximate $\Delta\delta$ of 0.7 ppm is noted for the inclusion of each quinolinone in **CB7**. Considering that the quinolinone

https://doi.org/10.1021/acsomega.5c03501
ACS Omega 2025, 10, 27550–27558

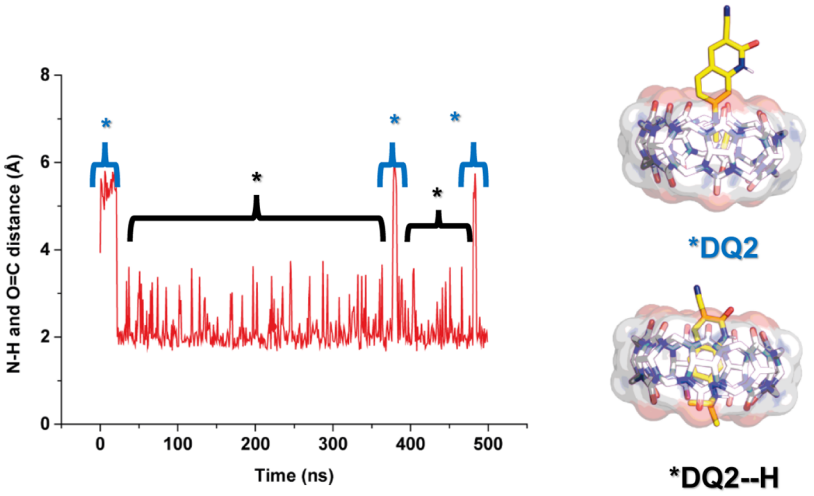

Figure 6. Distance obtained from amino N−H to the portal of **CB7** for protonated **DQ2**. A representative conformation is shown at the right of the graph.

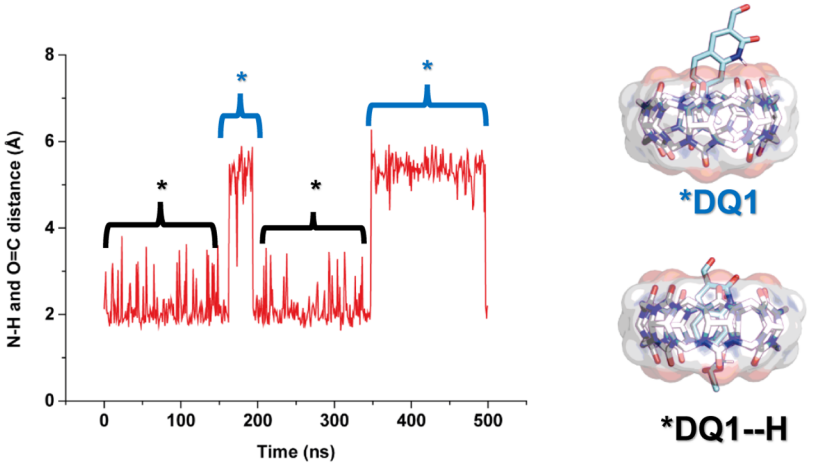

Figure 7. Distance obtained from amino N−H to the portal of **CB7** for protonated **DQ1**. A representative conformation is shown at the right of the graph.

is partially included, and for a deeper inclusion, like MV inside CB7, a $\Delta\delta$ of 1.5 ppm is observed,[47] our MD results correlate well with experimental evidence and previously reported $-NEt_2$-containing molecules with $\Delta\delta$ values ranging from 0.6 to 0.8 ppm.[35,36,46] Subsequently, we conducted simulations for the protonated probes; in Figures S19 and S20, an example of the conformation obtained from this study is shown. As observed, both probes are included in the macrocycle via the aromatic side of their core. However, the **DQ2** probe is slightly more included than **DQ1**, favoring the hydrogen bond between the lactam N−H and the upper carbonylic portal, as well as the N−H from $-NEt_2$ and the lower cucurbituril rim. A distance measurement between the amino N−H and the portals of the macrocycle during the MD suggests that the **DQ2** probe is more likely to form a hydrogen bond, as shown in Figure 6. In contrast, for **DQ1**, there are fractions of the simulations where this hydrogen bond is not favored, and the $-NEt_2$ moiety resides in the middle of the cavity (see Figure 7). Additionally, as illustrated in Figures 6 and 7, the protonated amino group is held inside the cavity of the macrocycle, which suggests that it is not stabilized by the solvent. Thus, the equilibrium is shifted toward the unprotonated quinolinone.

On the other side, the thermodynamic parameters of the complexes were determined using isothermal titration calorimetry (ITC) (see Figure 8), and the results are summarized in Table 2. Due to the poor water solubility of **DQ1** and **DQ2**, we used a 99:1 water:acetonitrile mixture for the macrocycle and the probes. In both cases, the binding is driven by enthalpy, which can be attributed to the release of high-energy water from the macrocycle cavity upon the inclusion of the probe.[48] On the other hand, the K_b values from ITC experiments are in good agreement with the constants obtained by fluorescence for both **DQ1** and **DQ2**.

Considering the modulation of the probe's properties upon the formation of supramolecular complexes, the significant increment in ϕ_f of **DQ2** allows us to select it as an indicator for displacement assay. To this end, we study methyl viologen (**MV**), a well-known pesticide, and the supramolecular complex **DQ2•CB7**. Upon the addition of **MV**, the fluorescence intensity decreases due to the liberation of **DQ2** and the formation of the **MV•CB7** complex. This variation allowed us to determine the binding affinity of **MV** toward **CB7**, as shown in Figure 9 with a value of 1.88×10^7 M^{-1}, in contrast with the reported in literature $\sim 10^5$ M^{-1} in buffer solution[47,49,50] and 10^6 M^{-1} in water.[50−52] Competitive

https://doi.org/10.1021/acsomega.5c03501
ACS Omega 2025, 10, 27550−27558

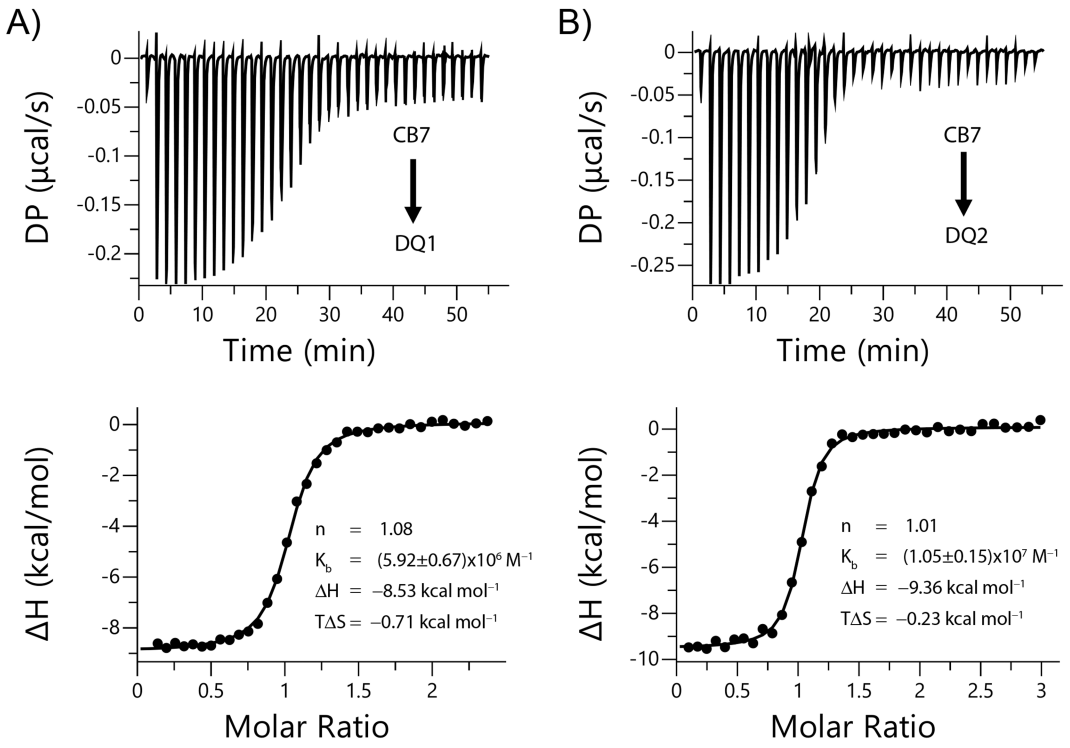

Figure 8. Representative enthalpogram for the binding between **CB7** (100 μM) and (A) **DQ1** (20 μM) and (B) **DQ2** (18.7 μM) in water:ACN (99:1) at 25 °C.

Table 2. Thermodynamic Data and Affinity Constant of DQ1 and DQ2 with CB7

	ΔH^a (kcal/mol)	$-T\Delta S^a$ (kcal/mol)	ΔG^a (kcal/mol)	ΔG^b (kcal/mol)	$K_b{}^a$ ($\times 10^{-6}$)	$K_b{}^c$ ($\times 10^{-6}$)	$K_{theo}{}^b$ ($\times 10^{-12}$)
DQ1•CB7	−8.53	−0.71	-9.2 (±0.1)	−17.17	5.9 (±0.7)	7.5 (±0.8)	3.27
DQ2•CB7	−9.36	−0.23	-9.6 (±0.1)	−18.23	10.5 (±1.6)	11.1 (±0.8)	19.14

[a]Values obtained from ITC. [b]Values obtained from MD. [c]Values obtained from fluorescence.

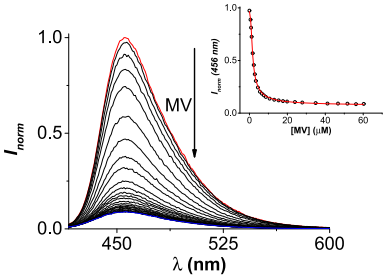

Figure 9. Indicator displacement assay (IDA) using the complex **DQ2•CB7** adding methyl viologen (**MV**) as a competitor ($K_{b\ MV\bullet CB7}$ = 1.88 × 10^7 M^{-1}) in water:ACN (99:1) at 25 °C.

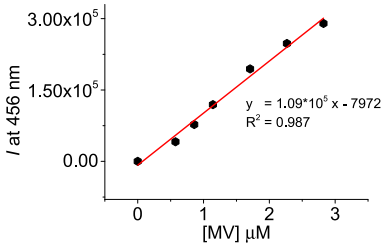

Figure 10. Linear range of the indicator displacement assay (IDA) using complex **DQ2•CB7** adding methyl viologen (**MV**) as a competitor in water:ACN (99:1) at 25 °C.

titration (see Figure 10) can be used to quantify the analyte in a range of 0.5 to 3 μM with a limit of detection of 0.24 μM. Considering these promising results, we can propose **DQ2** as a fluorescent probe useful for IDA.

CONCLUSIONS

We synthesized and characterized two quinoline-2(1*H*)-one derivatives and studied their optical properties and inclusion in the cucurbit[7]uril cavity. The formation of these supramolecular complexes leads to a modulation in the properties of the quinolinones, increasing the fluorescent quantum yield of the probes and allowing us to determine their affinity toward the macrocycle. This inclusion induces the largest negative ΔpK_a reported to date for 1:1 cucurbituril host−guest complexes. The thermodynamic results showed enthalpy-driven binding due to the liberation of high-energy water and a small entropy gain. Computational results are well correlated with the experimental binding affinity behavior. Finally, the modulation of optical properties and the excellent thermodynamic response toward the inclusion of the probes inside **CB7** allow us to propose the quinoline-2(1*H*)-one derivative **DQ2** as a new probe for indicator displacement assays.

EXPERIMENTAL SECTION

Materials. Reagents and materials were purchased from Sigma-Aldrich. Curcurbit[7]uril stock was prepared in ultra-

https://doi.org/10.1021/acsomega.5c03501
ACS Omega 2025, 10, 27550−27558

pure water (Milli-Q), and the concentration was determined by titration with cobaltocenium cation[53] by UV−vis spectroscopy.

Synthesis and Characterization of 7-(Diethylamino)-quinoline-2(1*H*)-one-3-carbaldehyde (DQ1). **DQ1** synthesis was carried out according to the methodology reported by Samaan et al.[31] A mixture of **1** (3.8 mmol, 0.99 g) and 40 mL of 70% aqueous acetic acid was refluxed for 4 h (Scheme 1). The reaction mixture was then allowed to cool to room temperature and poured into ice water. The resulting solid was filtered and washed with several portions of cold water. Finally, the product was purified by column chromatography using dichloromethane:methanol (30:1) as the eluent, yielding a yellow solid (0.65 g, 70% yield). ^{1}H NMR (400 MHz, CD_3CN) δ 9.95 (s, 1H), 8.29 (s, 1H), 7.57 (d, J = 9.2 Hz, 1H), 6.80 (d, J = 9.3 Hz, 1H), 6.42 (s, 1H), 3.46 (q, J = 6.9 Hz, 4H), 1.16 (t, J = 2.0 Hz, 6H). ^{13}C NMR (101 MHz, $CDCl_3$) δ 188.97, 164.92, 152.25, 144.10, 142.01, 132.17, 119.35, 110.39, 110.36, 94.73, 44.96, 12.55. HRMS m/z $[M + H]^+$ calculated for $C_{14}H_{16}N_2O_2$ 245.1284; found: 245.1290.

Synthesis and Characterization of 7-(Diethylamino)-quinoline-2(1*H*)-one-3-carbonitrile (DQ2). The **DQ2** probe was obtained as described by Chill and Mebane[54] for the transformation of aldehydes to nitriles. A mixture of **DQ1** (0.4 mmol, 98 mg), hydroxylamine chloride (0.76 mmol, 53 mg), and 2 mL of DMSO was added. The solution is stirred at 100 °C for 2 h, and then, the mixture is cooled to room temperature. The product is extracted with ethyl acetate (3 × 15 mL) and dried with anhydrous sodium sulfate. Then, the solvent was dried under vacuum, and the solid was purified by column chromatography with ethyl acetate as the eluent, yielding 86 mg of a yellow solid (90% yield). ^{1}H NMR (400 MHz, CD_3CN) δ 9.51 (s, 1H), 8.07 (s, 1H), 7.40 (d, J = 9.2 Hz, 1H), 6.73 (dd, J = 9.1, 2.5 Hz, 1H), 6.40 (d, J = 2.5 Hz, 1H), 3.48 (q, J = 7.1 Hz, 4H), 1.23 (t, J = 7.1 Hz, 6H). ^{13}C NMR (101 MHz, CD_3CN) δ 159.91, 152.38, 147.80, 143.00, 130.49, 117.00−116.00, 109.96, 109.12, 97.65, 94.29, 44.60, 11.71. HRMS m/z $[M + H]^+$ calculated for $C_{14}H_{14}N_3O$ 242.1293; found 242.1288.

Nuclear Magnetic Resonance (NMR) Studies. ^{1}H and ^{13}CNMR spectra were obtained at 25 °C by using a Bruker Avance 400 MHz spectrometer. NMR spectra were processed with MestreNova v14.2 software. Both probes DQ1 and DQ2 were characterized in acetonitrile-d_3, while the complexes DQn•CB7 were prepared by dissolving the probe and the macrocycle in a 1:1 mixture of acetonitrile-d_3 (ACN-d_3) and water-d_2 (D_2O).

High-Resolution (HR) QTOF-MS Studies. Mass spectrometry (HR-MS) experiments were conducted using a compact QTOF (Bruker) with an ionization voltage of 6 kV and negative polarity. The scan parameters were as follows: mass range: 50−3000 m/z, spectra rate: 2 Hz, capillary voltage: 6000 V, nebulizer: 0.6 bar, dry gas: 5 L/min, dry temp: 200 °C.

Spectroscopic Experiments. UV−vis spectroscopy was conducted using a Cary 60 spectrometer from Agilent Technologies. Similarly, fluorescence spectroscopy was measured using a Horiba FluoroMax-4 fluorescence spectrometer. Both measurements were performed at T = 25.0 ± 0.1 °C by using quartz cuvettes with an optical path length of 1 cm and a probe concentration of 1−2 μM.

Time-Resolved Fluorescence Measurements. Fluorescence lifetimes were measured using a Lifespec II picosecond fluorescence lifetime spectrometer from Edinburgh Instruments. We use a 458 nm laser diode as an excitation source and a fast red-sensitive PMT detector. A total of 10,000 counts were collected to determine the fluorescence lifetime at the fluorescent λ_{max} of each system. The instrument response function (IRF) was recorded by using a diluted Ludox solution to scatter the excitation light. A deconvolution of the IRF alongside the fluorescence decay was performed to obtain the fluorescence lifetimes.[8]

Determination of Fluorescent Quantum Yield (ϕ_f). The fluorescent quantum yield was determined using Coumarin-153 in ethanol as a standard (ϕ_s = 0.53).[55] The dependence of the absorbance and fluorescent emission is recorded for the probes and the standard. Then, using eq 2, quantum yield was obtained:[55]

$$\phi_x = \phi_s \left(\frac{Grad_x}{Grad_s}\right)\left(\frac{n_x^2}{n_s^2}\right) \tag{2}$$

with x and s being indices for the probe and the standard, respectively, $Grad$ is the gradient between the integrated fluorescent emission and the absorbance, η is the refractive index, and ϕ_s is the quantum yield of the standard. The emission was recorded by exciting at 410 nm with a slit width of 2 nm/2 nm for both the probes and the reference.

Determination of Binding Affinity Determination (K_b). The binding affinity was determined using a 1:1 model fitting by fluorescence spectroscopy, according to the equilibrium:

$$H + G \rightleftarrows HG \tag{3}$$

H corresponds to the host and G is the guest, while HG is the complex. Considering that,

$$K_b = \frac{[HG]_{Eq}}{[H]_{Eq} \times [G]_{Eq}} \tag{4}$$

We can obtain the following quadratic equation for 1:1 model binding:

$$[HG]_{Eq}^2 - \left([H]_T + [G]_T + \frac{1}{Ks}\right)[HG]_{Eq} + [H]_T[G]_T = 0 \tag{5}$$

where $[HG]_{Eq}$ corresponds to the complex in equilibrium and $[H]_T$ and $[G]_T$ are the total host and guest, respectively.

$$X_{HG} \times I_{HG} + X_G \times I_G = I_{calc} \tag{6}$$

with X being the molar fraction and I being the emission intensity of the complex (HG) and the guest (G). Finally, using eq 6, we can fit the experimental data by minimizing the difference between I_{calc} and the experimental emission (I_{exp}).

Determination of K_b by Isothermal Titration Calorimetry (ITC). Microcalorimetric experiments were carried out using a PEAQ-ITC instrument from Malvern Panalytical. The binding heats between **CB7** and **DQ1** and **DQ2** were studied in water:acetonitrile (99:1) at 25 °C. Data were processed using the PEAQ-ITC Analysis Software, and the integrated heat data were analyzed using ITC data-fitting software.

Indicator Displacement Assay (IDA). The competitive assay was carried out using 1,1'-dimethyl-4,4'-bipyridinium (**MV**) as a guest and **DQ2** as an indicator. The binding constant was calculated according to the reactions:

$$H + I \overset{K_1}{\rightleftarrows} HI + G \overset{K_2}{\rightleftarrows} HG + I \tag{7}$$

https://doi.org/10.1021/acsomega.5c03501
ACS Omega 2025, 10, 27550−27558

which can be used to derive the following expression using the relevant equilibrium and mass balance equations:

$$K_2^2[HI]_{Eq}^3 + (2K_2 + K_1 - K_2K_1[H]_T - 3K_2K_1[I]_T)[HI]_{Eq}^2 + (K_2K_1[H]_T[I]_T - K_1[H]_T - K_{s1}[I]_T - K_2K_1[I]_T^2 - 1)[HI]_{Eq} + K_1[H]_T[I]_T = 0 \quad (8)$$

where K_1 and K_2 are the binding constants of the indicator and the guest toward the host, respectively.

$$\frac{[HI]_{Eq} \times I_{HI} + [I]_{Eq} \times I_I}{[I]_T} = I_{calc} \quad (9)$$

The resolution of eq 8 allows the determination of $[HI]$ (and consequently $[I]$) values, which are required to calculate I_{calc} using eq 9. Minimizing the difference between I_{exp} and I_{calc} allows us to fit the experimental data and optimize the binding constant of **CB7** toward **MV**.

Computational Methods. The geometry of the molecules was optimized by density functional theory (DFT) at the B3LYP level of theory with the basis set 6-31+G(d,p) in the software Spartan'14.[56] The probe•**CB7** complexes were generated by molecular docking using the AutoDock 4.0 suite.[57] The grid map is centered on the macrocycle with dimensions of 30 × 30 × 30 points and a grid spacing of 0.375 Å. The calculations are based on the Lamarckian genetic algorithm, employing a population size of 150, a maximum of 2.5×10^6 energetic evaluations, a maximum of 27000 generations, a mutation rate of 0.02, and an exchange rate of 0.80. The more stable complexes were selected for subsequent molecular dynamics studies.

The former complexes were solvated in a periodic box of explicit TIP3P water. The simulation time was 300 ns for each system. Periodic boundary conditions were applied to the system in the direction of the three coordinates. The simulations were carried out under NTP conditions at 1 atm and 300 K. The software Amber18[58] suite with the AMBER FF14SB force field was used, and the parametrization was done using Antechamber and the LEaP module from AmberTools.[58]

The theoretical binding constants were obtained by a thermodynamic cycle through the molecular mechanical Poisson−Boltzmann surface area (MMPBSA) method of AMBER MD. This methodology considers the solvation of the probe, the macrocycle, and the complex, using the equation:

$$\Delta G^\circ_{bind,solution} = \Delta G^\circ_{bind,void} + \Delta G^\circ_{solv,comp} - (\Delta G^\circ_{solv,probe} + \Delta G^\circ_{solv,macro}) \quad (10)$$

with $\Delta G_{solv,\,comp}$, $\Delta G_{solv,\,probe}$, and $\Delta G_{solv,\,macro}$ being the Gibbs free energy of solvation for the complex, the probe, and the macrocycle, respectively, while $\Delta G_{bind,\,void}$ and $\Delta G_{bind,\,solution}$ are the binding free energy for the probe-macrocycle complex in void and solution, respectively.[59] It is important to mention that enthalpy and entropy were considered in these methods; however, as is known, the entropy value is usually overestimated. Thus, our calculation explicitly approximated the entropy.[60,61]

■ ASSOCIATED CONTENT

Supporting Information

The Supporting Information is available free of charge at https://pubs.acs.org/doi/10.1021/acsomega.5c03501.

Additional information on characterization and computational studies is available in Supporting Information in Figures S1−S20 and Table S1−S4 (PDF)

■ AUTHOR INFORMATION

Corresponding Author

Margarita E. Aliaga − *Departamento de Química Física, Escuela de Química, Facultad de Química y de Farmacia, Pontificia Universidad Católica de Chile, Santiago 7820436, Chile;* orcid.org/0000-0002-4143-0301; Email: mealiaga@uc.cl

Authors

Kevin Droguett − *Departamento de Química Física, Escuela de Química, Facultad de Química y de Farmacia, Pontificia Universidad Católica de Chile, Santiago 7820436, Chile;* orcid.org/0000-0002-7313-0864

Guillermo E. Quintero − *Departamento de Química Física, Escuela de Química, Facultad de Química y de Farmacia, Pontificia Universidad Católica de Chile, Santiago 7820436, Chile;* orcid.org/0000-0002-3634-9867

Nuno Basilio − *REQUIMTE/LAQV, Departamento de Química, Faculdade de Ciências e Tecnologia, Universidade Nova de Lisboa, Monte de Caparica 2829-516, Portugal;* orcid.org/0000-0002-0121-3695

Angélica Fierro − *Departamento de Química Orgánica, Escuela de Química, Facultad de Química y de Farmacia, Pontificia Universidad Católica de Chile, Santiago 7820436, Chile;* orcid.org/0000-0002-6507-4188

Edwin G. Pérez − *Departamento de Química Orgánica, Escuela de Química, Facultad de Química y de Farmacia, Pontificia Universidad Católica de Chile, Santiago 7820436, Chile*

Complete contact information is available at: https://pubs.acs.org/10.1021/acsomega.5c03501

Author Contributions

K.D. was involved in investigation, formal analysis, theoretical and experimental investigation, data curation, and writing of the original draft. G.E.Q. was involved in experimental investigation, data curation, and writing of the original draft. N.B. provided overall direction and coordination in some experiments (ITC and TRF) and contributed to the discussion of the manuscript. A.F. designed theoretical studies (molecular dynamics). E.P. synthesized validation. M.E.A. conceived the project, provided overall direction and coordination, contributed to manuscript preparation, and obtained financial support. All authors contributed to the review of the data and approved manuscript submission.

Notes

The authors declare no competing financial interest.

■ ACKNOWLEDGMENTS

This work was supported by Fondecyt grants N° 1210751 (**MEA**) and 1221030 (**AF**). **KD** acknowledges the ANID Doctoral Fellowship Folio N° 21210424. **GEQ** acknowledges the ANID Doctoral Fellowship Folio N° 21210698. Support from the Associate Laboratory for Green Chemistry-LAQV

(projects UIDB/50006/2020 and UIDP/50006/2020), financed by national funds from FCT/MCTES, is also acknowledged.

REFERENCES

(1) Oshovsky, G. V.; Reinhoudt, D. N.; Verboom, W. Supramolecular Chemistry in Water. *Angew. Chem. Int. Ed.* **2007**, *46* (14), 2366−2393.
(2) Wang, D.-X.; Wang, M.-X. Exploring Anion−π Interactions and Their Applications in Supramolecular Chemis.try. *Acc. Chem. Res.* **2020**, *53* (7), 1364−1380.
(3) Williams, G. T.; Haynes, C. J. E.; Fares, M.; Caltagirone, C.; Hiscock, J. R.; Gale, P. A. Advances in Applied Supramolecular Technologies. *Chem. Soc. Rev.* **2021**, *50* (4), 2737−2763.
(4) Bhadra, B. N.; Shrestha, L. K.; Ma, R.; Hill, J. P.; Yamauchi, Y.; Ariga, K. Metal−Organic Framework on Fullerene (MOFOF) as a Hierarchical Composite by the Integration of Coordination Chemistry and Supramolecular Chemistry. *ACS Appl. Mater. Interfaces* **2024**, *16* (31), 41363−41370.
(5) Farcas, A.; Liu, Y.-C.; Nilam, M.; Balan-Porcarasu, M.; Ursu, E.-L.; Nau, W. M.; Hennig, A. Synthesis and Photophysical Properties of Inclusion Complexes between Conjugated Polyazomethines with γ-Cyclodextrin and Its Tris-O-Methylated Derivative. *Eur. Polym. J.* **2019**, *113*, 236−243.
(6) Marcos, P. M.; Berberan-Santos, M. N. Recent Advances in Calixarene-Based Fluorescent Sensors for Biological Applications. *Sensors* **2024**, *24* (22), 7181.
(7) Liu, D.; Du, J.; Qi, S.; Li, M.; Wang, J.; Liu, M.; Du, X.; Wang, X.; Ren, B.; Wu, D.; Shen, J. Supramolecular Nanoparticles Constructed from Pillar[5]Arene-Based Host−Guest Complexation with Enhanced Aggregation-Induced Emission for Imaging-Guided Drug Delivery. *Mater. Chem. Front.* **2021**, *5* (3), 1418−1427.
(8) Zúñiga-Núñez, D.; Mura, F.; Mariño-Ocampo, N.; Zúñiga, B.; Robinson-Duggon, J.; Zamora, R. A.; Poblete, H.; Aspée, A.; Fuentealba, D. Exploring the Photophysics of Cinnamoyl-Coumarin Derivatives in Cucurbit [7]Uril Complexes and Assessing Phototoxicity in HeLa Cells. *Dyes Pigm.* **2024**, *229*, 112290.
(9) Droguett, K.; Quintero, G. E.; Santos, J. G.; Aliaga, M. E. Advancement in Supramolecular Control of Organic Reactivity Induced by Cucurbit[n]Urils. *J. Incl. Phenom. Macrocycl. Chem.* **2023**, *103* (1−2), 1−20.
(10) Assaf, K. I.; Tehrani, F. N.; Quintero, G. E.; Hein, R.; Aliaga, M. E.; Nau, W. M. Regioselective Dimerizati.on of Methylcyclopentadiene inside Cucurbit[7]Uril. *Chem. − Eur. J.* **2025**, *31* (12), No. e202403964.
(11) Fierro, A.; García-Río, L.; Arancibia-Opazo, S.; Alcázar, J. J.; Santos, J. G.; Aliaga, M. E. Cucurbit[7]Uril as a Supramolecular Catalyst in Base-Catalyzed Reactions. Experimental and Theoretical Studies on Carbonate and Thiocarbonate Hydrolysis Reactions. *J. Org. Chem.* **2021**, *86* (2), 2023−2027.
(12) Barooah, N.; Kunwar, A.; Khurana, R.; Bhasikuttan, A. C.; Mohanty, J. Stimuli-Responsive Cucurbit[7]Uril-Mediated BSA Nanoassembly for Uptake and Release of Doxorubicin. *Chem. -Asian J.* **2017**, *12* (1), 122−129.
(13) Liang, L.; Peng, T.; Geng, X. Y.; Zhu, W.; Liu, C.; Peng, H.-Q.; Chen, B. Z.; Guo, X. D. Aggregation-Induced Emission Photosensitizer Microneedles for Enhanced Melanoma Photodynamic Therapy. *Biomater. Sci.* **2024**, *12* (5), 1263−1273.
(14) Chiangraeng, N.; Nakano, H.; Nimmanpipug, P.; Yoshida, N. Selective Molecular Recognition of Amino Acids and Their Derivatives by Cucurbiturils in Aqueous Solution: An MD/3D-RISM Study. *J. Mol. Liq.* **2023**, *386*, 122503.
(15) Xu, P.; Zhou, S.; Druzhinin, S. I.; Schönherr, H.; Song, B. Design of a PH-Sensitive Supramolecular Fluorescent Probe for Selective Cancer Cell Imaging. *Dyes Pigm.* **2023**, *217*, 111366.
(16) Zhang, S.; Grimm, L.; Miskolczy, Z.; Biczók, L.; Biedermann, F.; Nau, W. M. Binding Affinities of Cucurbit[*n*]Urils with Cations. *Chem. Commun.* **2019**, *55* (94), 14131−14134.
(17) Alnajjar, M. A.; Nau, W. M.; Hennig, A. A Reference Scale of Cucurbit[7]Uril Binding Affinities. *Org. Biomol. Chem.* **2021**, *19* (39), 8521−8529.
(18) Zhang, G.; Emwas, A.-H.; Shahul Hameed, U. F.; Arold, S. T.; Yang, P.; Chen, A.; Xiang, J.-F.; Khashab, N. M. Shape-Induced Selective Separation of Ortho-Substituted Benzene Isomers Enabled by Cucurbit[7]Uril Host Macrocycles. *Chem* **2020**, *6* (5), 1082−1096.
(19) Alcázar, J. J.; Márquez, E.; García-Río, L.; Robles-Muñoz, A.; Fierro, A.; Santos, J. G.; Aliaga, M. E. Changes in Protonation Sites of 3-Styryl Derivatives of 7-(Dialkylamino)-Aza-Coumarin Dyes Induced by Cucurbit[7]Uril. *Front. Chem.* **2022**, *10*, 10.
(20) Aliaga, M. E.; De la Fuente, J. R.; García-Río, L.; Rojas-Romo, C.; Uribe, I.; Díaz-Hernández, D.; Fierro, A.; Cañete, A. Modulation of Lactam-Lactim Tautomerism of Quinoxalin-2-one Induced by Cucurbit[7]Uril: A Comparative Study with Oxazin-2-one. *ChemistrySelect* **2018**, *3* (39), 10999−11007.
(21) Miskolczy, Z.; Biczók, L. Kinetics and Thermodynamics of Berberine Inclusion in Cucurbit[7]Uril. *J. Phys. Chem. B* **2014**, *118* (9), 2499−2505.
(22) Anjanikar, S. S.; Chandole, S. S. Anti-Microbial Study and Synthesis of Schiff Bases of 3-Actyl 4-Hydroxy Quinolin-2-One. *Orient. J. Chem.* **2023**, *39* (1), 197−201.
(23) Doan, N. Q. H.; Tran, H. N.; Nguyen, N. T. M.; Pham, T. M.; Nguyen, Q. D. K.; Vu, T.-T. Synthesis, Antimicrobial - Cytotoxic Evaluation, and Molecular Docking Studies of Quinolin-2-one Hydrazones Containing Nitrophenyl or Isonicotinoyl/Nicotinoyl Moiety. *Chem. Biodiversity* **2024**, *21* (10), No. e202401142.
(24) Abdo Moustafa, E.; Abdelrasheed Allam, H.; Fouad, M. A.; El Kerdawy, A. M.; Nasser Eid El-Sayed, N.; Wagner, C.; Abdel-Aziz, H. A.; Abdel Fattah Ezzat, M. Discovery of Novel Quinolin-2-One Derivatives as Potential GSK-3β Inhibitors for Treatment of Alzheimer's Disease: Pharmacophore-Based Design, Preliminary SAR, in Vitro and in Vivo Biological Evaluation. *Bioorg. Chem.* **2024**, *146*, 107324.
(25) Elbastawesy, M. A. I.; El-Shaier, Y. A. M. M.; Ramadan, M.; Brown, A. B.; Aly, A. A.; Abuo-Rahma, G. E.-D. A. Identification and Molecular Modeling of New Quinolin-2-One Thiosemicarbazide Scaffold with Antimicrobial Urease Inhibitory Activity. *Mol. Diversity* **2021**, *25* (1), 13−27.
(26) El-Aal, R. M. A.; Koraierm, A. I. M. S. Absorption Spectra Studies and Biological Activity of Some Novel Conjugated Dyes. *J. Chin. Chem. Soc.* **2000**, *47* (2), 389−395.
(27) Fabian, W. M. F.; Niederreiter, K. S.; Uray, G.; Stadlbauer, W. Substituent Effects on Absorption and Fluorescence Spectra of Carbostyrils. *J. Mol. Struct.* **1999**, *477* (1−3), 209−220.
(28) Paul, N.; Jiang, M.; Bieniek, N.; Lustres, J. L. P.; Li, Y.; Wollscheid, N.; Buckup, T.; Dreuw, A.; Hampp, N.; Motzkus, M. Substituting Coumarins for Quinolinones: Altering the Cycloreversion Potential Energy Landscape. *J. Phys. Chem. A* **2018**, *122* (38), 7587−7597.
(29) Cisse, L.; Djande, A.; Capo-Chichi, M.; Delatre, F.; Saba, A.; Tine, A.; Aaron, J.-J. Revisiting the Photophysical Properties and Excited Singlet-State Dipole Moments of Several Coumarin Derivatives. *Spectrochim. Acta, Part A* **2011**, *79* (3), 428−436.
(30) Chamlagai, D.; Bora, P.; Bhatta, A.; Upadhyaya, J.; Phanrang, P. T.; Bora, U.; Mitra, S. Donor-Acceptor Functionalized Coumarin Derivatives: Synthesis, Fluorescence Modulation, Interaction with Human Serum Albumin and Acetylcholinesterase Inhibition Activity. *J. Photochem. Photobiol. A Chem.* **2024**, *447*, 115273.
(31) Samaan, G. N.; Wyllie, M. K.; Cizmic, J. M.; Needham, L.-M.; Nobis, D.; Ngo, K.; Andersen, S.; Magennis, S. W.; Lee, S. F.; Purse, B. W. Single-Molecule Fluorescence Detection of a Tricyclic Nucleoside Analogue. *Chem. Sci.* **2021**, *12* (7), 2623−2628.
(32) Lin, H.; Zhou, Z.; Ma, X.; Chen, Q.; Han, H.; Wang, X.; Qi, J.; Yang, Y. One Pot Synthesis of Aryl Nitriles from Aromatic Aldehydes in a Water Environment. *RSC Adv.* **2021**, *11* (39), 24232−24237.
(33) Quintero, G. E.; Espinoza, C.; Valencia, J.; Insuasty, D.; Tiznado, W.; Leiva-Parra, L.; Santos, J. G.; Pérez, E. G.; Aliaga, M. E.

https://doi.org/10.1021/acsomega.5c03501
ACS Omega 2025, 10, 27550−27558

Quinolin-2(1 *H* -)-One-Isoxazole Dye as an Acceptor for Mild Addition of Bisulfite in Cationic or Zwitterionic Aqueous Micellar Solutions. *New J. Chem.* **2024**, *48* (40), 17605−17615.
(34) Zhang, C.; Sun, Y.; Wang, J.; He, Y.; Zhang, Y.; Zhang, L.; Song, F. Synthesis and Application of Quinolinone Derivative Fluorescent Probe for High Selective Detection of Hg2+. *Chem. J. Chin. Univ.* **2020**, *41* (8), 1785−1791.
(35) Aliaga, M. E.; García-Río, L.; Pessêgo, M.; Montecinos, R.; Fuentealba, D.; Uribe, I.; Martín-Pastor, M.; García-Beltrán, O. Host−Guest Interaction of Coumarin-Derivative Dyes and Cucurbit[7]Uril: Leading to the Formation of Supramolecular Ternary Complexes with Mercuric Ions. *New J. Chem.* **2015**, *39* (4), 3084−3092.
(36) Ahmed, S. A.; Seth, S.; Gautam, R. K.; Seth, D. Inclusion of a Coumarin Derivative inside the Macrocyclic Hosts: A Spectroscopic, Thermodynamic and Theoretical Investigation. *J. Mol. Liq.* **2018**, *264*, 550−562.
(37) Chatterjee, A.; Maity, B.; Seth, D. Supramolecular Interaction between a Hydrophilic Coumarin Dye and Macrocyclic Hosts: Spectroscopic and Calorimetric Study. *J. Phys. Chem. B* **2014**, *118* (32), 9768−9781.
(38) Gupta, M.; Maity, D. K.; Nayak, S. K.; Ray, A. K. Modulation of Photophysics and Photostability of Cationic Coumarin 1 Dye upon Inclusion with Macrocyclic Host Cucurbit[7]Uril. *J. Photochem. Photobiol. A Chem.* **2015**, *300*, 15−21.
(39) Sedgwick, A. C.; Brewster, J. T.; Wu, T.; Feng, X.; Bull, S. D.; Qian, X.; Sessler, J. L.; James, T. D.; Anslyn, E. V.; Sun, X. Indicator Displacement Assays (IDAs): The Past, Present and Future. *Chem. Soc. Rev.* **2021**, *50* (1), 9−38.
(40) Barooah, N.; Mohanty, J.; Pal, H.; Bhasikuttan, A. C. Non-Covalent Interactions of Coumarin Dyes with Cucurbit[7]Uril Macrocycle: Modulation of ICT to TICT State Conversion. *Org. Biomol. Chem.* **2012**, *10* (26), 5055−5062.
(41) Koner, A. L.; Nau, W. M. Cucurbituril Encapsulation of Fluorescent Dyes. *Supramol. Chem.* **2007**, *19* (1−2), 55−66.
(42) Barooah, N.; Mohanty, J.; Bhasikuttan, A. C. Cucurbituril-Based Supramolecular Assemblies: Prospective on Drug Delivery, Sensing, Separation, and Catalytic Applications. *Langmuir* **2022**, *38* (20), 6249−6264.
(43) Wang, C.; Chi, W.; Qiao, Q.; Tan, D.; Xu, Z.; Liu, X. Twisted Intramolecular Charge Transfer (TICT) and Twists beyond TICT: From Mechanisms to Rational Designs of Bright and Sensitive Fluorophores. *Chem. Soc. Rev* **2021**, *50* (22), 12656−12678.
(44) Sinn, S.; Krämer, J.; Biedermann, F. Teaching Old Indicators Even More Tricks: Binding Affinity Measurements with the Guest-Displacement Assay (GDA). *Chem. Commun.* **2020**, *56* (49), 6620−6623.
(45) Trevisan, A.; Ferreira, A. S. D.; Marrec, P.; Parola, A. J.; Basílio, N. Tuning the Sign and Magnitude of Complexation-Induced p K_a Shifts in Cucurbit[7]Uril Host-Guest Complexes by Molecular Engineering. *Isr. J. Chem.* **2024**, *64*, 6−7.
(46) Basílio, N.; Gago, S.; Parola, A. J.; Pina, F. Contrasting p K_a Shifts in Cucurbit[7]Uril Host−Guest Complexes Governed by an Interplay of Hydrophobic Effects and Electrostatic Interactions. *ACS Omega* **2017**, *2* (1), 70−75.
(47) Kim, H.-J.; Jeon, W. S.; Ko, Y. H.; Kim, K. Inclusion of Methylviologen in Cucurbit[7]Uril. *Proc. Int. Acad. Sci.* **2002**, *99* (8), 5007−5011.
(48) Biedermann, F.; Uzunova, V. D.; Scherman, O. A.; Nau, W. M.; De Simone, A. Release of High-Energy Water as an Essential Driving Force for the High-Affinity Binding of Cucurbit[*n*]Urils. *J. Am. Chem. Soc.* **2012**, *134* (37), 15318−15323.
(49) Ling, Y.; Mague, J. T.; Kaifer, A. E. Inclusion Complexation of Diquat and Paraquat by the Hosts Cucurbit[7]Uril and Cucurbit[8]-Uril. *Chem. − Eur. J.* **2007**, *13* (28), 7908−7914.
(50) Zhang, X.; Xu, X.; Li, S.; Li, L.; Zhang, J.; Wang, R. A Synthetic Receptor as a Specific Antidote for Paraquat Poisoning. *Theranostics* **2019**, *9* (3), 633−645.
(51) Pavez, P.; Fierro, A.; Rojas, M.; García-Rio, L.; Dinamarca-Villarroel, L.; Fuentealba, D.; Droguett, K.; Santos, J. G.; Aliaga, M. E. A Comparative Study on the Cucurbit[7]Uril-based Indicator Displacement Assay for Methyl Viologen. A Theoretical and Experimental Perspective. *J. Phys. Org. Chem.* **2024**, *37* (7), No. e4581.
(52) Qing, T.; Jing, Z.; Gui-xian, S.; Yun-yun, X.; Ying, H.; Zhu, T.; Qing-di, Z.; Gang, W. A Fluorescent Probe Based Host-Guest Complexation between Cucurbit[7]Uril and Neutral Red for the Detection of Paraquat Herbicide in Water Sample. *Spec. Spectral Anal.* **2018**, *38* (4), 1160−1164.
(53) Yi, S.; Kaifer, A. E. Determination of the Purity of Cucurbit[*n*]Uril (*n* = 7, 8) Host Samples. *J. Org. Chem.* **2011**, *76* (24), 10275−10278.
(54) Chill, S. T.; Mebane, R. C. A Facile One-Pot Conversion of Aldehydes into Nitriles. *Synth. Commun.* **2009**, *39* (20), 3601−3606.
(55) Würth, C.; Grabolle, M.; Pauli, J.; Spieles, M.; Resch-Genger, U. Relative and Absolute Determination of Fluorescence Quantum Yields of Transparent Samples. *Nat. Protoc.* **2013**, *8* (8), 1535−1550.
(56) Shao, Y.; Molnar, L. F.; Jung, Y.; Kussmann, J.; Ochsenfeld, C.; Brown, S. T.; Gilbert, A. T. B.; Slipchenko, L. V.; Levchenko, S. V.; O'Neill, D. P.; et al. Advances in methods and algorithms in a modern quantum chemistry program package. *Phys. Chem. Chem. Phys* **2006**, *8* (27), 3172.
(57) Morris, G. M.; Huey, R.; Lindstrom, W.; Sanner, M. F.; Belew, R. K.; Goodsell, D. S.; Olson, A. J. Autodock4 and AutoDockTools4: automated docking with selective receptor flexiblity. *J. Comput. Chem.* **2009**, *30* (16), 2785−2791.
(58) Case, D. A.; Ben-Shalom, I. Y.; Brozell, S. R.; Cerutti, D. S.; Cheatham, T. E., III; Cruzeiro, I. W. D.; Darden, T. A.; Duke, R. E.; Ghoreishi, D.; Gilson, M. K., et al. *AMBER 2018*; University of California: San Francisco, 2018.
(59) Wang, C.; Greene, D.; Xiao, L.; Qi, R.; Luo, R. Recent Developments and Applications of the MMPBSA Method. *Front. Mol. Biosci.* **2018**, *4*, 4.
(60) Ekberg, V.; Ryde, U. On the Use of Interaction Entropy and Related Methods to Estimate Binding Entropies. *J. Chem. Theory Comput.* **2021**, *17* (8), 5379−5391.
(61) Genheden, S.; Ryde, U. The MM/PBSA and MM/GBSA Methods to Estimate Ligand-Binding Affinities. *Expert Opin. Drug Discovery* **2015**, *10* (5), 449−461.

https://doi.org/10.1021/acsomega.5c03501
ACS Omega 2025, 10, 27550−27558